JCTC Journal of Chemical Theory and Computation

Article

pubs.acs.org/JCTC

Transmembrane Permeation Mechanism of Charged Methyl Guanidine

Yukun Wang,[†] Dan Hu,*[,‡] and Dongqing Wei*[,†]

[†]State Key Laboratory of Microbial Metabolism and College of Life Sciences and Biotechnology, Shanghai Jiao Tong University, Shanghai 200240, People's Republic of China

[‡]Department of Mathematics, Institute of Natural Sciences, and MOE-LSC, Shanghai Jiao Tong University, Shanghai 200240, People's Republic of China

Supporting Information

ABSTRACT: The mechanism of transmembrane ion permeation is studied using charged methyl guanidine as a model ion. With a widely applied reaction coordinate, our umbrella sampling results reveal a significant finite-size effect in small simulation systems and a serious hysteresis in large systems. Therefore, it is important to re-examine the simulation techniques for studying transmembrane permeation mechanism of ions suggested in previous works. In this work, two novel collective variables are designed to acquire a continuous trajectory of the permeation process and small statistical errors through umbrella sampling. A water-bridge mechanism is discussed in detail. In this mechanism, a continuous water chain (or a chain of water molecules and lipid head groups) is formed across the membrane to conduct the transmembrane permeation of charged methyl guanidine. We obtain a continuous transition trajectory by combining the two-dimensional umbrella sampling in the local region of the saddle state and a one-dimensional sampling in the out region. Our free energy analysis shows that, with the presence of the water bridge, the energy barrier of the transmembrane permeation of ions is reduced significantly. Our analysis suggests that the water-bridge mechanism is common for permeation of ions across thick membranes, including palmitoyloleoyl phosphocholine and dipalmitoylphosphatidylcholine membranes.

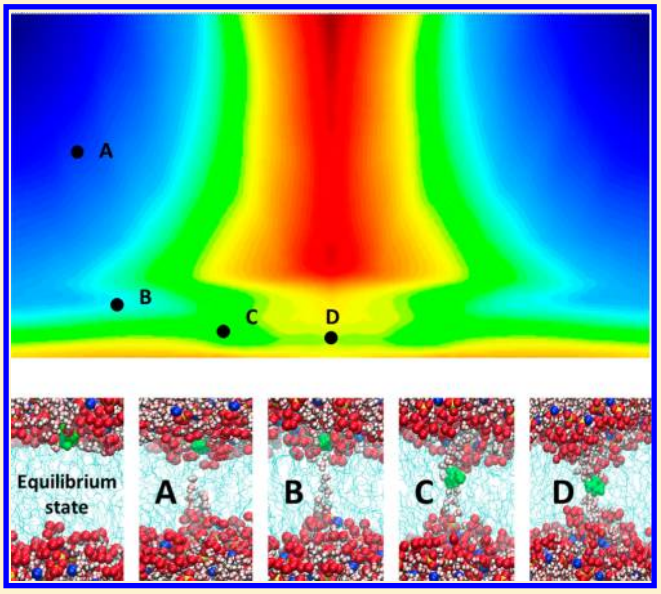

INTRODUCTION

A lipid bilayer provides an osmotic barrier for a cell or a cellular organelle to prevent its content from freely escaping and protects it from constant attacking of environmental molecules. This important function is mainly achieved by the hydrophobic core that generates a high energy barrier for the transmembrane permeation of charged and hydrophilic groups.[1,2] However, many of the membrane functions are also performed by breaking the integrity of the membrane. For example, the function of many membrane proteins and membrane-active antimicrobial peptides, such as Melittin[3] and Magainin,[4] are closely related to transmembrane insertion of charged groups. A detailed study on the mechanism of the permeation process of charged and hydrophilic groups across and partitioning into a lipid bilayer is important in understanding the function of membrane-active proteins and peptides. Knowledge of the permeation processes is also helpful in designing new ways for drug delivery and designing new membrane-active drugs, such as antimicrobial peptides and their mimics.[5,6]

There is a long history of the study on transmembrane permeation of charged particles. The transmembrane permeation rates of ions (H^+, Na^+, and Cl^-) through different types of membranes were studied using different experimental methods.[7−10] Permeation rates were shown to be significantly dependent on membrane thickness and environmental condition. In the experimental studies of membrane peptides, such as antimicrobial peptides, charged groups are also suggested to be able to achieve a transmembrane permeation to form complicated transmembrane structures.[11,12] A few transmembrane permeation mechanisms, such as the water-pore mechanism, has been proposed in explaining the above experimental results.[13] However, it is hard to obtain the detailed mechanism of the transmembrane permeation process by experiments, mainly because these processes are rare events

Received: August 19, 2013
Published: March 12, 2014

dx.doi.org/10.1021/ct400738r | J. Chem. Theory Comput. 2014, 10, 1717−1726

that rarely happen in the microscopic time scale, but once the transition happens, it is finished very quickly.[14]

Molecular dynamics (MD) simulations, in particular, when combined with sampling methods such as umbrella sampling,[15] are helpful in obtaining the details of rare events. Transmembrane permeation of ions,[14,16−20] transmembrane insertion of peptides with charged groups,[21,22] flip-flop of lipids,[23−25] and formation of water pore in a membrane[26] were simulated by a few groups. The membrane thickness is suggested to be important in determining transmembrane permeation mechanisms, a water pore mechanism for thin membranes and dehydration mechanism (or referenced as the solubility−diffusion mechanism) for thick membranes.[16−19,27,28] In most of the simulations, the reaction coordinate is selected to be the relative height of the center of mass of an ion or a charged (hydrophilic) group to the horizontal center plane of the hydrophobic core of the membrane.[14,16−25] Using this reaction coordinate, transition trajectories and potential of mean forces (PMF) of these processes are obtained with umbrella sampling. As a result of large dehydration energy,[29] ions usually keep their solvation shells during the whole permeation processes.[14,21] However, when the membranes are very thick, a dehydration mechanism can also by employed.[17,19,27] It is also reported that, when the ions or charged groups are restrained at the center of the hydrophobic core, they connect to only one hydrophobic−hydrophilic interface of the membrane (in this work, an "interface" is defined by the oxygen atoms of lipid molecules in a single monolayer).[14,30] In particular, when the membrane is thick, the transitions of such configurations to their mirror configurations (in which the ion is attached to the other interface) are rarely observed in simulations. From this point of view, part of the transition trajectory and the saddle state of the transition are not observed in existing works. As evidence of this fact, there is a sharp peak in the PMF profiles obtained from umbrella samplings with this reaction coordinate.[14,16−18,21,30] Expensive two-dimensional umbrella sampling[21] is also performed near the saddle state, aiming to remove the sharp peak and find the saddle state, but the water pore configuration that is suggested in experiments is not observed in these simulations.

Water-pore configurations are found in the study of flip-flop of lipids[23,24] and the water-pore mechanism is suggested in transmembrane permeation of ions. However, the sharp peak in their PMF profiles[23,24] and the failure in finding the water-pore configuration in dioleoylphosphatidylcholine (DOPC) and palmitoyloleoyl phosphocholine (POPC) membranes[24] suggest that further efforts in understanding the mechanism are needed. In a recent work,[31] a random walk in the hyperplane normal to the reaction coordinate is used to find the water-pore configuration and obtain a smoother peak. In another recent work,[22] new reaction coordinates are employed to characterize the water pore at different stages of the permeation process and a PMF profile is obtained by patching umbrella sampling results with different reaction coordinates. This work provides clear evidence of the water pore assist mechanism in the transmembrane permeation process. In these works,[22,31] the detailed mechanism of forming a water pore is not discussed.

In this work, our main goal is to obtain a clear mechanism of the transmembrane permeation of ions. Charged methyl guanidine ($MguanH^+$) is used as a model ion. First, we reperformed the MD simulation of the transmembrane permeation of $MguanH^+$ through umbrella sampling with the widely applied reaction coordinate. We show that, for small-size simulation systems, the trajectory and the PMF suffer from a significant finite-size effect due to the periodic boundary condition in MD simulations; whereas for large-size simulation systems, there is a jump of the configuration and a serious hysteresis in the permeation trajectory. Therefore, an improvement in sampling technique is necessary for our study. We solved this problem mainly by designing tailored reaction coordinates.

Then, by designing a second reaction coordinate, our simulation shows that a water bridge (which can be a pure water chain or a mixed polar chain of water molecules and lipid head groups) is formed to decrease the energy barrier. However, in these simulations, we can also observe frequent jumps between the water-bridge configuration and the non-water-bridge configuration. Therefore, we designed a third reaction coordinate to capture this jump. A two-dimensional umbrella sampling is performed at the local region where configuration jumps are observed frequently. With the two-dimensional sampling, a continuous trajectory of the permeation process is obtained and the statistical errors become very small because all significant configuration jumps are avoided.

On the basis of our simulation results, the full permeation process of $MguanH^+$ can be summarized as the following: driven by thermal fluctuations, first, a symmetric deformation of the two lipid monolayers leads to a decrease in local membrane thickness near to the ion; next, a water chain is sprouted from one monolayer and reaches the other, forming a bridge across the membrane at this local region (the bridge can be a mix of water molecules and lipid head groups); then, the ion moves across the membrane along the bridge; finally, the bridge breaks and the system relaxes to the other equilibrium state. Compared to previous water-pore mechanisms,[23,24,31,22] our two-dimensional energy surface clearly shows the origin of the hysteresis. In our mechanism, the water pore is formed at a much smaller membrane deformation than that in previous works[23,24,31,22] and the sharp peak of PMF is prevented because of the avoidance of hysteresis.

RESULTS

In this section, we first show the dilemma in the umbrella sampling with the widely used reaction coordinate, RC_1, the finite-size effect in small simulation systems and serious hysteresis in large simulation systems. Then, we show the umbrella sampling results with the new reaction coordinate, RC_2, in which the water-bridge configuration at the saddle state is observed. Finally, we designed a third reaction coordinate, RC_3, to acquire the formation of the water bridge. With the two-dimensional umbrella sampling using RC_2 and RC_3, we discuss the proper permeation process with the free energy surface. Although we can directly show the sampling results with RC_2 and RC_3, the result obtained with RC_1 is helpful in designing new reaction coordinates and understanding the sampling results obtained with RC_2 and RC_3.

Umbrella Sampling with RC_1. As is applied in previous works[14−18,21,23,24,30] and illustrated in Figure 1A, the relative height, $RC_1 = Z_{ion} - Z_C$, where Z_{ion} is the height of the center of mass of the $MguanH^+$ group and Z_C is the height of the horizontal center plane of the lipid bilayer, is used as the reaction coordinate to perform umbrella sampling. The PMF profiles obtained through the umbrella samplings are shown in Figure 2. The PMF is significantly greater in System42 (the number denotes the number of POPC molecules in the

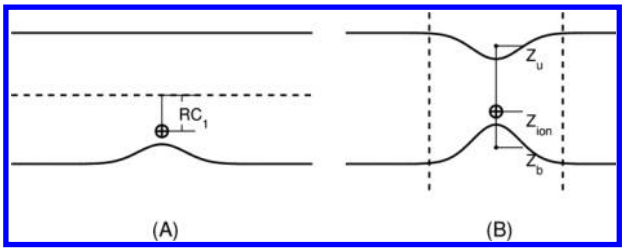

Figure 1. Illustration of the two reaction coordinates. In both figures, the upper and bottom solid lines represent the two hydrophobic−hydrophilic interfaces of the membrane (defined by the oxygen atoms of the lipid molecules) and the sign "⊕" represents the ion. In panel A, the dash line represents the center plane of the membrane. In panel B, the two small dots represent the weighted mass center in the local cylinder confined in the dashed lines.

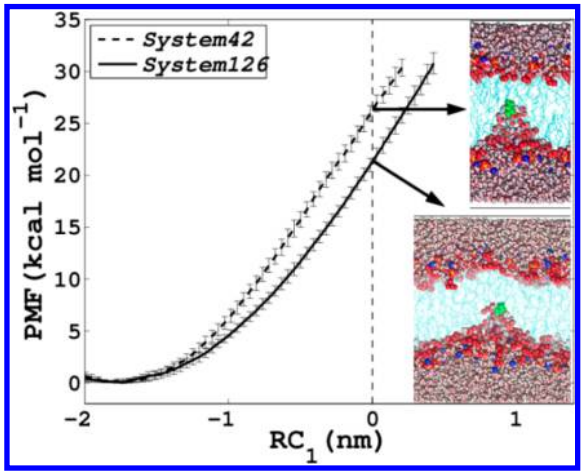

Figure 2. PMF profiles and the statistical errors obtained by umbrella sampling with RC_1. The two curves are the PMF profiles of System42 and System126, respectively. Snapshots of configurations for System42 and System126 for $RC_1 = 0$ are shown on the right. The upper interface is planar in System42 but has a submissive deformation in System126. In the snapshots in this work, the ion $MguanH^+$ is shown in green; the oxygen atoms of POPC and carbonyl groups, the phosphorus atoms, and the nitrogen atoms are shown by red, tan, and blue spheres, respectively; the water molecules are shown by small pink and white spheres; the hydrocarbon tails of POPC molecules are shown by cyan lines.

system) than in System126. As has been demonstrated in previous works,[14,30] the interface of the membrane follows all the way to the center of the membrane. As a result of this large deformation, the periodic boundary condition in MD simulations leads to a significantly higher deformation energy in a smaller system (shown in Figure 2). In other words, the finite-size effect brings a nonphysical constraint to the simulation and generates significant errors in the PMF profile and the transition trajectory.

To remove the finite-size effect, our first idea is to simply increase the size of the simulation box. However, in this case, we are forced to face a serious hysteresis. As is shown in Figure 2, the PMF obtained from a 100 ns sampling is an increasing function of the reaction coordinate RC_1 in the neighboring windows of Window-0 (the number shows the target value of the external harmonic potential for RC_1). Note that there are two metastable states under the umbrella potential in these windows, the ion attaching to the upper or the lower interfaces, respectively. However, a considerable energy barrier between the two metastable states prevents the system from a quick transition from one configuration to the other. This introduces hysteresis in umbrella sampling. In System42, a transition is observed in Window-0 in about 100 ns whereas, in System126, no transition is observed in Window-0 during 200 ns of simulation. The statistical errors are smaller than 1.0 kcal/mol in both System42 System126. The error in both systems are much smaller than the difference of the two PMF profiles. The statistical error is consistent with that observed in previous work.[32] The size effect is shown to be insignificant for the flip-flop of lipids in dimyristoylphosphatidylcholine (DMPC) membranes, in which a water pore is formed when the lipid head is fixed at the center of the membrane.[25] The reason that the water pore can form may be the big size of the lipid head and the small thickness of DMPC membrane, both of which effectively reduce the distance between the lipid head and the opposite interface.

Due to the serious hysteresis, the transition trajectory cannot be properly found using umbrella sampling with RC_1. Similar observations are also found in the previous umbrella samplings with RC_1.[14,16−18,21,30] In particular, the important saddle state of the permeation process is not captured. If we make use of the symmetry of the system to generate a symmetric PMF, a considerable additional energy barrier in Window-0 between the two metastable states is neglected and the PMF profiles of the transmembrane permeation processes contain a sharp peak at Window-0.

Now we fall into a dilemma. Using a small system, the PMF is both overestimated due to the constraint of periodic boundary condition and underestimated due to the loss of the additional energy barrier in Window-0; however, using a large system, the serious hysteresis also prevent us from obtaining the transition trajectory and the accurate energy barrier. In fact, in both situations, we are not able to get the continuous transition trajectory and the saddle state of the permeation process.

A detailed study on the origin of the hysteresis in large systems helps in designing a new reaction coordinate. As is shown in Figure 2, the upper interface appears differently in the small and large simulations systems, which is planar in small systems and bent submissively in large systems. This difference is also the result of the constraint of boundary condition. In the competition between the surface energy of the upper interface and the packing energy of the hydrophobic tails, the surface energy is more sensitive to the simulation size. As a result, the bending is prohibited in small systems but allowed in large systems. If the opposite interface needs to get close to the ion at the saddle state, the submissive bending makes it harder to reach the saddle state, and leads to a serious hysteresis in large systems. As a result of the energy barrier induced by large packing energy, the umbrella sampling with the reaction coordinate RC_1 fails to find the saddle state. In the study of the flip-flop of lipids,[17,21,23,27] the big size of the lipid head can reduce the distance between the lipid head and the opposite interface. As a result, the water pore configuration can form more easily.

Umbrella Sampling with RC_2. Apparently, the two hydrophobic−hydrophilic interfaces should be able to deform to get closer under the control of the new reaction coordinate. Under this requirement, we find a new reaction coordinate for our further umbrella sampling, $RC_2 = Z_u + Z_b - 2Z_{ion}$, where Z_u and Z_b are the z-coordinates of the locally weighted mass center of the upper and the bottom interfaces (we realize that RC_2 is

dx.doi.org/10.1021/ct400738r | J. Chem. Theory Comput. 2014, 10, 1717−1726

similar to the reaction coordinate used in a recent work[22]). In fact, when the ion is attached to one interface of the bilayer, e.g., the bottom interface, there is only a small change in the distance between the ion and the local interface, $Z_b - Z_{ion}$. As a result, RC_2 mainly describes the distance of the ion to its opposite interface. The geometrical meaning of RC_2 is illustrated in Figure 1.

The permeation trajectory is obtained with umbrella sampling using RC_2. As RC_2 increases from −4 nm to about −0.5 nm, the ion moves closer and closer to the center plane of the membrane. As we have expected in designing the new reaction coordinate, both the upper and the bottom interfaces moves toward the center plane. In the window that RC_2 is about ±0.5 nm, there are two metastable states under the external umbrella potential. As is shown in Figure 3, in one of the two states, a water bridge is formed (as is shown in Figure 1s in the Supporting Information, the water bridge can be either a chain of water molecules or a mixed chain of water molecules and lipid head groups). The water-bridge and non-water-bridge states also exist in a few nearby windows. About 10 times of forward and backward transitions between the two metastable states under the umbrella potential are observed in 120 ns of simulations. This suggests that the energy barrier and the energy difference between the two metastable states are small. As RC_2 becomes closer to zero, the probability that the system is in a water-bridge configuration becomes larger. This indicates that the water-bridge configuration begins to have a lower free energy. In the two windows that RC_2 is about ±0.2 nm, the water-bridge configuration becomes the only stable configuration in System126 and System256, suggesting a large difference in free energy of the two states. Therefore, we can draw the conclusion that the water-bridge mechanism is favorable in the permeation process of $MguanH^+$. At the saddle state, we have $RC_2 = 0$ and the ion moves to the center of the water bridge.

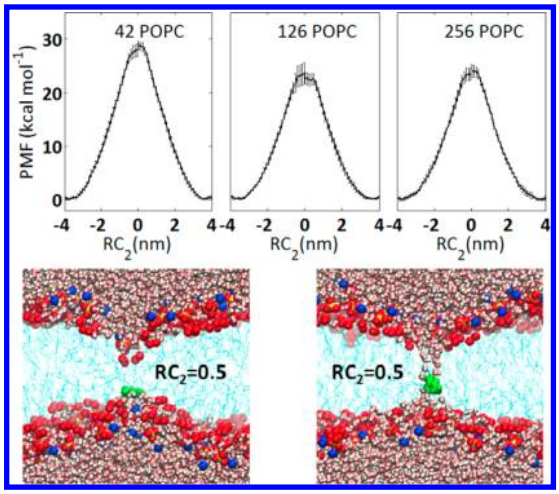

Figure 3. PMF profiles with error bars obtained in System42, System126, and System256 using the new reaction coordinate RC_2 and the snapshots of two metastable configurations with and without a water bridge. The PMF are integrated both −4 to 0 nm and from +4 to 0 nm so that we can compare the statistical error.

The PMF profiles obtained with the umbrella sampling using RC_2 are shown in Figure 3. There is no longer a sharp peak in the PMF profiles. The free energy barrier (relative free energy difference of the saddle state to the equilibrium state) is almost the same for System126 and System256 but about 4.5 kcal/mol smaller than that of System42. Therefore, the size effect is negligible in systems with 126 or more lipid molecules. The phenomenological results obtained with RC_2 are consistent with previous work on DOPC membranes[22] because the reaction coordinates are similar. The statistical errors in all three systems are smaller than 1.0 kcal/mol in the out region ($|RC_2| > 0.8$ nm) and can have a significant increase at about $|RC_2| = 0.5$ nm to be more than 1.0 kcal/mol, although we have paid more simulation time in the inner region ($|RC_2| < 0.8$ nm). The error analysis clearly shows that the configuration jump between the two metastable states is the origin of big statistical errors.

Two-Dimensional Umbrella Sampling. Because there is still a jump between configurations with and without a water bridge, further efforts in acquiring the continuous permeation trajectory and reducing the statistical error are needed. A new collective variable, RC_3, is designed to capture this transition. A full definition of RC_3 is included in the Methods section. The reaction coordinate RC_3 describes the continuity of the water bridge, namely, it is small for continuous water bridge and large for broken water chain. For a broken water chain, RC_3 is almost the length (projected in the z-direction) of the gap. As shown in Figure 4, RC_3 can be used to separate well the water-bridge configurations and the non-water-bridge configurations. To obtain a continuous transition trajectory, we perform a two-dimensional umbrella sampling with RC_2 and RC_3 around the saddle state.

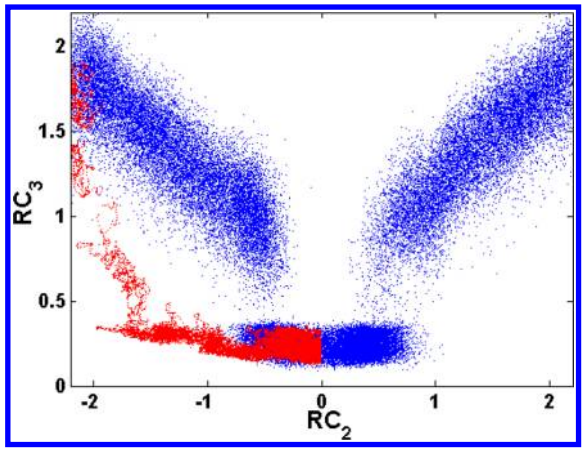

Figure 4. Phase plane illustration of the trajectories obtained in umbrella sampling with RC_2 (blue) and in an unbiased MD simulation starting from the saddle state (red). There is a jump in the trajectories obtained in umbrella sampling at $RC_2 \approx 0.5$. The big difference between the blue and the red trajectories shows another significant hysteresis.

Our next problem is to determine the ranges of the two reaction coordinates to perform the two-dimensional umbrella sampling. We performed 40 unbiased MD simulations starting from the saddle state. The initial configurations are randomly selected from the window with $RC_2 \approx 0$ in the umbrella sampling using RC_2. The system quickly reaches the equilibrium state in which the membrane is planar and the ions lies in one of the two interfaces. One relaxation trajectory is shown in Figure 4 (in the Supporting Information, we have plotted all the trajectories on the phase plane in Figure 2s). According to the trajectory, the relaxation process involves two stages: the ion first moves on the water bridge to one of the

interfaces, then the water bridge is broken and the membrane becomes planar. In most of the simulations, when the water bridge is broken, RC_2 has a value between 1.0 and 2.0 nm. A big difference can be observed between the umbrella sampling results and the unbiased MD simulation results on the phase plane in Figure 4. Therefore, the hysteresis is also serious in the umbrella sampling with RC_2, although the energy barrier is already small to allow frequent jumps between the metastable states. In our MD simulations, the system starting from the saddle states reaches at the equilibrium states in about 3.1 ns on average. This time scale is much smaller than that of the lifetime of transient water pores reported in previous works, in which a complete membrane defect is formed and the relaxation time is 10−100 ns .[33,34] This quick relaxation suggests that there is no significant free energy barrier in breaking the water bridge in the unbiased MD simulations. On the basis of the MD simulation trajectories, the two-dimensional umbrella sampling is performed in the domain $[-2.1,0] \times [0.1,1.3]$.

The free energy surface obtained from the two-dimensional umbrella sampling is shown in Figure 5A. Near saddle state D is

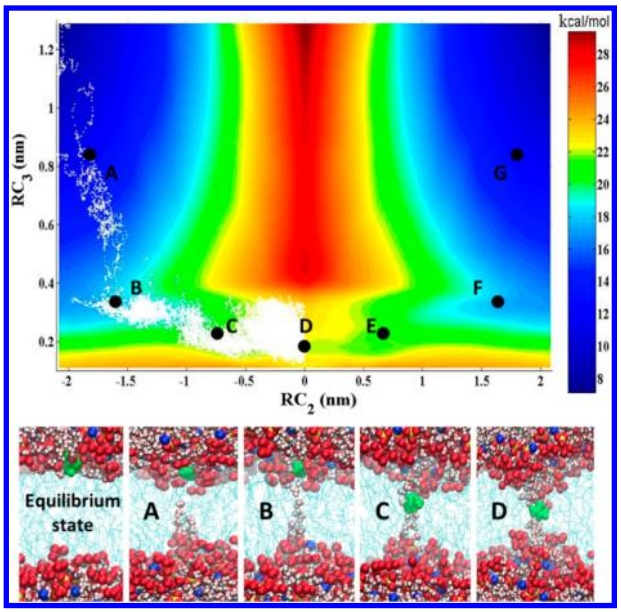

Figure 5. Free energy surface obtained with umbrella sampling in System126 and snapshots of typical configurations on the transition path. The white points in the free energy surface are obtained from an unbiased MD simulation starting at saddle state D. The configurations E, F, and G and the other equilibrium state can be obtained by the mirror configurations of C, B, and A and the equilibrium state above, respectively.

a ravine in the energy surface, which corresponds to a water-bridge configuration, which links the two free energy basins near to the equilibrium states, providing the transition path from one equilibrium state to the other. The free energy density near the saddle state is about 22.2 kcal/mol, whereas the free energy density of the saddle state in the non-water-bridge transition is greater than 29 kcal/mol. This big difference in free energy density suggests that the water bridge is crucial in the ion-permeation process. Because the ravine is narrow, the effective free energy barrier of the permeation process is about 23.0 kcal/mol, including the contribution of configuration entropy. This free energy barrier is smaller than that obtained with the umbrella sampling using RC_2, which is about 24.2 kcal/mol as shown by the PMF in Figure 3 (note that a local free energy barrier of about 1.5 kcal/ml between the water-bridge configuration and non-water-bridge configuration is already lost in this energy barrier). Compared to the non-water-bridge mechanism, the reduction in the energy barrier is more than 6 kcal/mol with the presence of the water bridge. Because all the significant configuration jumps are avoided, the statistical errors of the two-dimensional sampling are smaller than 0.7 kcal/mol (see Figure 3s in the Supporting Information).

A trajectory of the MD simulation begin at the saddle state is shown on the free energy surface by the white points in Figure 5A. Comparing the trajectory points and the free energy surface, we can draw the conclusion that the relaxation process from the saddle state to the equilibrium state roughly follows the minimal free energy path, which is the most possible transition path.[35] On the basis of the transition path theory, most transition paths lie in a tube near the minimal free energy path.[35] More relaxation trajectories from the saddle state are shown in the phase plane of RC_2 and RC_3 (Figure 2s in the Supporting Information) and the paths really exist in a transition tube.

Typical configurations of the permeation process are shown in Figure 5B. The thermal-driven permeation process of $MguanH^+$ involves four stages: first, both interfaces of the bilayer deform locally toward the center plane; second, a water chain is sprouted from one interface and reaches the other, forming a water bridge; third, the ion moves along the water bridge to the other interface; fourth, the water bridge breaks and the system relaxes to the equilibrium state.

In the previous work,[21] a two-dimensional umbrella sampling is also used to find the transition trajectory and reduce the statistical error in the transmembrane permeation of a protonated arginine side chain in a transmembrane helix. We have the same start point in designing new reaction coordinates by using the information of configuration jumps. The work on protonated arginine has more emphasis on the pose change of the side chain. According to our study, the deformation of the opposite interface and the formation of the water chain may also be important in these permeation processes.

Consistent with the above permeation mechanism, the free energy barrier can also be divided into three parts, the energy cost in membrane deformation, in forming the water bridge, and in moving the ion to the middle of the water bridge. According to our simulation results, the energy cost in deformation of the two symmetric monolayers can be well approximated by a harmonic potential, $k_d d^2$, where d is the deformation of a single monolayer and $k_d \approx 24.0$ kcal/nm^2 is the elastic modulus, whereas the energy cost in forming a water bridge can be approximated by $\gamma(h - 2d) + 2E_s$, where $\gamma \approx 7.5$ kcal/nm is the line tension of the water bridge, h is the thickness of the membrane hydrophobic core, which is about 2.2 nm for POPC lipid membranes at 310 K, and E_s is the energy cost in forming a singular point that links the water bridge and a membrane interface. By minimizing the total energy cost in deformation and in forming a water bridge, one can find that the water bridge is formed when the deformation of the membrane is about 0.31 nm, which is consistent with configuration A in Figure 5 and much smaller than that is shown in Figure 3. In the relaxation processes from the saddle state, when the water bridge is broken, RC_2 can have a value of about 1.0 to 2.0 nm. The deformation on both side can be about 0.2 to 0.6 nm, which is consistent with that obtained

from the energetic analysis. The deformation can be directly measured from the simulation results and the upper bound can be estimated by $(h - RC_2)/2$, where $h \approx 2.2$ nm is the core thickness of the POPC membrane. Our analysis shows that the three parts of energy cost are about 2.4, 15.7, and 5.1 kcal/mol, respectively; a large energy amount is the cost of forming a water bridge to avoid a large deformation of the membrane, which is more costly in energy. In particular, the free energy in forming a water bridge is 18.1 kcal/mol, which is consistent with previous results.[23,26] Note that the optimal deformation, $d = (\gamma/k_d)$, depends only on the elastic modulus and the line tension. Therefore, a decrement (increment) in membrane thickness directly reduces (increases) the length of the water bridge, leading to a significant decrement (increment) in the free energy barrier of the transmembrane permeation of ions.

The deformation is small (0.31 nm) in the minimal energy path when the water chain begins to form. From the viewpoint of least action,[35,36] the minimal energy path has the least action and the maximal probability density among all paths with the same free energy barrier. What's more, most transition paths lie in a tube along the minimal energy path. However, it does not mean that this small deformation is sufficient to induce the formation of a water chain. For example, in our umbrella sampling with RC_2, the water chain begins to form only when RC_2 is as small as 0.5 nm (the deformation is about 0.85 nm). In fact, when RC_2 is small, the non-water-bridge configuration has a smaller free energy and the water bridge will not be formed.

In the non-water-bridge mechanism, the energy barrier is mainly due to the large deformation energy. For example, for POPC membranes, there is a deformation of half the membrane thickness (about 1.1 nm) at the saddle state. The energy barrier estimated from the deformation energy is about 29.0 kcal/mol, which is consistent with our sampling results. When the reduction in membrane thickness is very large and the core thickness of the membrane is very small, e.g., 1.8 nm, the deformation energy in the non-water-bridge mechanism is significantly reduced and the energy barrier of the non-water-bridge mechanism becomes smaller than the water-bridge mechanism. In this case, the water bridge may be no longer necessary in the permeation process.

For very thick membranes, a dehydration mechanism is suggested in the previous work[17−19,27] in which the hydration defect of the ion can be broken and an isolated ion−water complex is formed to pass through the membrane. In fact, the energy barrier of the water-bridge mechanism almost increases linearly with the membrane thickness due to the energy cost in forming a water bridge, but the dehydration mechanism has a glass ceiling for the energy barrier of ion permeation in membranes with different thicknesses. Therefore, the dehydration mechanism will be employed in the ion permeation through very thick membranes. In this case, both RC_1 and RC_2 can be used in umbrella sampling to find the saddle state at which the isolated ion−water complex is in the middle of the membrane. However, for ion permeation in a membrane with a medium thickness, both mechanisms can be found with RC_2 but the water-bridge mechanism cannot be found with RC_1.

Because the first two parts of the free energy costs depend little on the type of the monovalent cation and the third part is not very large, the difference in the free energy barrier of different monovalent cations may be small. This observation is consistent with previous simulation results on $MguanH^+$ and protonated methylammonium ($MamH^+$).[18] Thus, the permeability, P, of ions (such as sodium ion Na^+) can be estimated using the energy barrier we obtained

$$P \approx \frac{h}{k_b e^{\Delta G/k_B T}}$$

where $h \approx 1$ nm is the effective thickness in which ions are interacting with the membrane (the membrane interfacial energy for Na^+ is small), $k_b \approx 3.1$ ns is the relaxation time from saddle state to the equilibrium state, $\Delta G \approx 23$ kcal/mol is the free energy barrier, k_B is the Boltzmann constant, and $T = 310$ K is the temperature. The permeability, P, is on the magnitude of 10^{-14} cm/s, which is 2 orders of magnitude smaller than the permeability of potassium ion measured in POPC membranes.[9]

Stability of the Water Bridge. There are a series of experimental and theoretical studies on whether the water-bridge (also referenced as water-pore[23,24,31,22,26] or prepore[37]) configuration is a metastable state. The metastability is supported by conductance experiments in which transmembrane ion flux come as bursts rather than single events.[37] Dynamic loading experiments[38] are also fitted well by a model with the assumption of metastable water-bridge configuration. However, previous free energy calculation of transmembrane pore formation process[26] does not support the existence of this metastability. Below, we consider the metastability of the water bridge based on our simulation results.

On the free energy surface in Figure 5, we can see a ridge that separates the water-bridge configurations and the non-water-bridge configurations. On the isosurface with fixed RC_2, the ridge provides an energy barrier between the two configurations. The presence of the ridge is the origin of the hysteresis in the umbrella sampling with RC_2. In the case that the abstract value $|RC_2| < 0.7$ nm, the water-bridge configurations have a lower free energy density comparing to the non-water-bridge configurations whereas, for $|RC_2| > 0.7$ nm, the water-bridge configurations have a higher free energy density. As $|RC_2|$ increases, the relative height of the ridge to the water-bridge configuration in the isosurface of fixed RC_2, which is the energy barrier to break the water bridge with fixed RC_2, becomes smaller and smaller and vanishes at about 1.6 nm (where the ion is off the bridge). This means that when the ion is on the water bridge, it is hard to break the bridge (with fixed RC_2) whereas, when the ion is off the bridge, there is almost no energy barrier to break the bridge. This is consistent with our MD simulation results in which the system relaxes quickly from the saddle state to the equilibrium state. Therefore, our umbrella sampling results suggest that the water-bridge configuration is not a metastable state for a POPC lipid membrane.

In fact, when the ion is on the bridge, it is always surrounded by water molecules to prevent it from being exposed to the hydrophobic environment. In particular, when the ion moves to the middle of the bridge, the whole water chain is separated into two parts, each of which has a small length. As a result, the water bridge is also thickened when the ion is on the bridge (shown in Figure 5). Both the shortening and the thickening effects of the water chain lead to an observable energy barrier to break the water bridge. On the contrary, when the ion is off the bridge, the water chain becomes long and thin, thus becomes easy to be broken. From this point of view, for a membrane with smaller thickness, such as a DMPC lipid membrane, the water bridge is shorter and thicker, and there may be an observable energy barrier in breaking the water bridge.

Therefore, according to our simulation results, the water-bridge configuration is not metastable for a POPC membrane but may be metastable for thinner membranes.

METHODS

Systems Setup and Simulation Details. POPC lipid membranes with different sizes were built up. In System42, there are 42 POPC molecules and 1466 water molecules; In System126, there are 126 POPC molecules and 4945 water molecules; In System256, there are 256 POPC molecules and 7702 water molecules. Each system also contains one $MguanH^+$ ion and one counterion, Cl^-. To check the influence of ion screening, in System126$^+$ (used in the Supporting Information), 20 Na^+ and 20 CL^- ions are added to System126.

All the MD simulations are performed using the GROMACS 4.0 (www.gromacs.org)[39] with NPT ensemble. OPLS-AA-compatible united-atom lipid parameters[40] and TIP3P water model[41] are used. The force field parameters for protonated methyl guanidine ($MguanH^+$) have been derived from OPLS all-atom (OPLS-AA) protein force field.[42] The van der Waals interactions are computed with a cutoff of 1 nm. Electrostatic interactions were calculated by PME.[43] Bonds involving hydrogen atoms are restrained using LINCS.[38,42] The integration time-step is set to be 2 fs and neighbor lists are updated every 5 steps. A heat bath is applied with time constant τ_T = 0.5 ps using Nosé−Hoover temperature coupling algorithm.[44] Atmospheric pressure is maintained using Parrinello−Rahman semi-isotropic pressure coupling method[45] with isotropic compressibility of 4.6 × 10^5 bar^{-1} and time constant τ_P = 5 ps.

Definition of Reaction Coordinates. As is shown in Figure 1, the relative height $Z_{ion} - Z_c$ between the center of mass of the $MguanH^+$ group, Z_{ion}, and the center plane of the lipid bilayer, Z_c, is widely used as the reaction coordinate (RC_1) to describe the permeation process of molecules through a lipid membrane. This reaction coordinate cannot control the distance between the ion and the opposite surface, which is the origin of the hysteresis in umbrella sampling with RC_1.

To make the opposite surface come closer to the ion when the ion moves to the center of the hydrophobic core, we designed a new reaction coordinates, $RC_2 = Z_u + Z_b - 2Z_{ion}$, where Z_u and Z_b are the weighted local heights of the upper and bottom interfaces defined by the oxygen atoms of lipid molecules, respectively. The local heights are defined as

$$Z_u = \sum_i \frac{1 + \cos(\alpha r_{i,u})}{\sum_j 1 + \cos(\alpha r_{j,u})} Z_{i,u}$$

and

$$Z_b = \sum_i \frac{1 + \cos(\alpha r_{i,b})}{\sum_j 1 + \cos(\alpha r_{j,b})} Z_{i,b}$$

where $\alpha = \pi$ nm^{-1} defines the cylindrical local region with the radius of 1 nm in which the oxygen atoms of lipid molecules are used to calculate the local heights, i and j are the indices of the oxygen atoms, u and b denote the upper and bottom interfaces, respectively, Z_i are the z-coordinates of the oxygen atoms, and r_i are the projected distances of the oxygen atoms to the center of mass of the $MguanH^+$ ion in the $x-y$ plane.

Another reaction coordinates, RC_3, is designed to describe the continuity of the water chain between the upper and bottom interfaces. Note that an incontinuous water chain has a big gap and the gap length can be used to describe the continuity. We first sort the oxygen atoms of lipid and water molecules with their z-coordinates between Z_b and Z_u. These small parts of oxygen atoms in the system are important in forming a water bridge. Note that we have included the oxygen atoms of lipid molecules because they can also contribute in forming hydrogen bonds. This allows the bridge to be a mixture of water molecules and lipid head groups. Then, the new reaction coordinate is defined as

$$RC_3 = [\sum_i (Z^s_{i,O} - Z^s_{i+1,O})^\beta]^{1/\beta}$$

where $\beta = 6$ and $Z^s_{i,O}$ are the z-coordinates of the oxygen atoms with the index i in the sorted order. Because the power β is big, the largest term in $|Z^s_{i,O} - Z^s_{i+1,O}|$ contributes a large part in RC_3. For example, if $|Z^s_{i,O} - Z^s_{i+1,O}|$ has twice the value of $|Z^s_{j,O} - Z^s_{j+1,O}|$, the contribution of $|Z^s_{i,O} - Z^s_{i+1,O}|$ in RC_3 is 64 times that of $|Z^s_{j,O} - Z^s_{j+1,O}|$. Therefore, a continuous water chain has a small value of RC_3, whereas a broken water chain has a large value. For an incontinuous water chain, RC_3 almost has the value of the gap length. In particular, when there is no water chain, RC_3 is almost the distance between the two interfaces at the local region. From this point of view, by controlling the value of RC_3 to be smaller and smaller, one can narrow the gap and make a continuous water bridge. When a continuous water chain is formed, RC_3 is already very small (about 0.3 nm). When the water chain becomes thicker, RC_3 can have an insignificant decrease.

Free Energy Calculation. In the one-dimensional umbrella samplings, the harmonic potentials $U_i(RC) = 1/2K_i(RC - RC_i)^2$ of elastic springs are used as the umbrella potential to keep the reaction coordinate RC around RC_{i0}, where i is the index of the sampling window and K_i is the elastic modulus. In umbrella sampling with RC_1, the sampling range of RC_1, [−2.0,0.6], is divided into 27 windows with the width of 0.1 nm and the elastic modulus K_i = 1500 kj·nm^{-2} is used in the umbrella sampling. For both System42 and System126, each window is simulated for 100 ns. In Window-0, a 120 ns simulation is performed in System42 and a 200 ns simulation is performed in System256. In the umbrella sampling with RC_2, the sampling range, [−4,4], is divided into two parts, the saddle region, [−0.8,0.8], and outer region, [−4,−0.8] and [0.8,4]. A relatively stiff elastic modulus K_i = 1000 kj·nm^{-2} and a window width of 0.1 nm are used in the saddle region and a relatively soft elastic modulus K_i = 400 kj·nm^{-2} and a window width of 0.2 nm are used in the outer region. The windows in saddle region are simulated for 300 ns in System42, 150 ns in System126, and 120 ns in System256. The windows in the outer region are simulated for 70 ns in all systems. In the two-dimensional umbrella sampling with RC_2 and RC_3, an array of 7 × 9 = 63 sampling windows cover the sampling range [−2.1,0] × [0.1,1.3]. In each window, it is equilibrated for 5 ns and then simulated for 40 ns.

The pull code has been implemented in standard GROMACS 4.0 and can be used to perform umbrella sampling with RC_1. In umbrella sampling with RC_2 and RC_3, harmonic potentials, $U_i(RC_a) = 1/2K_i(RC_a - RC_{ai})^2$, a = 2,3, are applied in window i with the target value of RC_{ai}. The force component introduced by the harmonic potentials on a coordinate x_j of the system can be calculated as

$$f_j = -K_i(\mathrm{RC}_a - \mathrm{RC}_{ai})\frac{\partial \mathrm{RC}_a}{\partial x_j}$$

Additional code to apply the forces is directly implemented in GROMACS in our simulation.

The PMFs (free energy surface) as a function of reaction coordinates are calculated by WHAM.[46] To obtain the statistical error in Figures 2 and 3, sampling results obtained with $RC_1$and RC_2 in each window are equally divided into 10 and 7 blocks, respectively. The standard variation of the PMFs of all but the first blocks is used as the statistical error in Figures 2 and 3. In particular, the PMF for the sampling results obtained with RC_2 are integrated both from −4 to 0 nm and from +4 to 0 nm, so that we can study the statistical error due to the configuration jumps. The free energy surface is obtained by combining the two-dimensional umbrella sampling and the umbrella sampling with RC_2 and the free energy density of the equilibrium state is set to be zero. The reaction coordinates RC_2 and RC_3 are nonlinear functions of the original position coordinates of the atoms, which may contribute errors in the PMF profiles due to the difference in the density of configurations. This density can be calculated by the ensemble average $\langle|(\partial \mathbf{C})/(\partial \mathrm{RC}_2)|\rangle$ and $\langle|((\partial \mathbf{C})/(\partial \mathrm{RC}_2)) \times ((\partial \mathbf{C})/(\partial \mathrm{RC}_3))|\rangle$, where $\mathbf{C}$ is the configuration vector, which denotes all the original position coordinates of atoms. However, according to our numerical results, both the two densities are very close to 0.5 in all the windows (only a few percentages of changes). This means that both RC_2 and RC_3 are pretty linear and the two tangential directions, $(\partial \mathbf{C})/(\partial \mathrm{RC}_2)$ and $(\partial \mathbf{C})/(\partial \mathrm{RC}_3)$, are almost perpendicular to each other. Therefore, we can neglect the difference in configuration density in our free energy calculation.

CONCLUSION AND DISCUSSION

We studied the transmembrane permeation mechanism of $MguanH^+$ by designing two novel reaction coordinates and combining the one-dimensional umbrella sampling and the two-dimensional umbrella sampling results to obtain a continuous trajectory and a local free energy surface. We have performed three umbrella samplings on the transmembrane permeation of the model ion, $MguanH^+$, using reaction coordinates, RC_1, RC_2, and the combination of RC_2 and RC_3. We pointed out the finite-size effect and the hysteresis in the umbrella sampling with the reaction coordinate RC_1 that is applied widely in previous studies. The simulation results obtained with RC_2 successfully find the saddle state of the permeation process, in which a water bridge is clearly observed. This result is similar to previous studies on DOPC membranes.[22] However, the permeation trajectory obtained from RC_2 is still not continuous because there is a configuration jump between the water-bridge configuration and the non-water-bridge configuration. Finally, with the two-dimensional umbrella sampling using RC_2 and RC_3 near the saddle state, the continuous transmembrane permeation trajectory of $MguanH^+$ is obtained. With the avoidance of significant configuration jumps, we have achieved a very small statistical error, which allows us to discuss the differences in energy barriers of different mechanisms. The permeation process driven by thermal fluctuations includes the following four stages: first, beginning at an equilibrium state, both interfaces of the bilayer deform locally toward each other; second, a water chain is generated from one of the interfaces and reaches the other, forming a water bridge; third, the ion steps onto the water bridge and moves to the other interface (in this case, the bridge can also become a mixing of water molecules and lipid head groups); fourth, the water bridge breaks and the system relaxes to the other equilibrium state. With the presence of a water bridge in transmembrane ion permeation, the free energy barrier is significantly reduced comparing to a non-water-bridge permeation mechanism, as suggested in previous works. Compared to previous works that also observed a water pore configuration,[23,24,31,22] our two-dimensional energy surface clearly show the origin of the hysteresis. In our mechanism, the water pore is formed at a small membrane deformation.

Although we only performed the sampling with POPC membranes, our decomposition of the free energy barrier is helpful in considering other membranes. The optimal deformation determined by the elastic modulus of deformation and the line tension of the water bridge is very small compared to the membrane thickness. As a result, a water bridge should also be important in the permeation of ions across membranes with slightly smaller thickness, such as dipalmitoylphosphatidylcholine or DMPC membranes, which have a core thickness of about 2.15 and 1.9 nm, respectively. With a similar two-dimensional umbrella sampling on such membranes, one should be able to obtain a similar free energy surface, with a ravine in the water-bridge configuration connecting the two basins near the equilibrium states and two ridges separating the water-bridge configurations and non-water-bridge configurations. For a membrane with a large core thickness (e.g., > 1.8 nm), the water-bridge configuration should also be the main mechanism for transmembrane permeation of other ions or transmembrane insertion of a peptide with charged (or highly hydrophilic) groups (for DMPC membranes, the difference in energy barrier of the two mechanisms may be small and both mechanisms can be chosen). For very thick membranes, the energy in forming a water bridge may become greater than the dehydration energy. In this case, a dehydration mechanism will be employed. Because most bio-membranes have a median thickness, the water-bridge mechanism is most important for the transmembrane permeation of cations. The reaction coordinates, RC_2 and RC_3, may also be applicable in other transmembrane processes including the transmembrane insertion of peptides.

ASSOCIATED CONTENT

Supporting Information

Three sections. The first shows that the water bridge can be a mix of water molecules and lipid head groups. The second shows the relaxation process from the saddle state in the phase plane. The last shows the convergence and the statistical error of the two-dimensional PMF. This material is available free of charge via the Internet at http://pubs.acs.org.

AUTHOR INFORMATION

Corresponding Authors

*D. Hu. E-mail: hudan80@sjtu.edu.cn.
*D. Wei. E-mail: dqwei@sjtu.edu.cn.

Notes

The authors declare no competing financial interest.

ACKNOWLEDGMENTS

This work was supported by NSFC grants 11004131, 91230202, 11174201, the National Basic Research Program of China (973 Program) 2012CB721000, the National High-

Tech R&D Program (863 Program Contract No. 2012AA020307), the Key Project of Shanghai Science and Technology Commission 11JC1406400, R&D grant AE0710005 from Shanghai Jiao Tong University, Ph.D. Programs Foundation of Ministry of Education of China (Contract No., 20120073110057), and HPC π of Shanghai Jiao Tong University.

REFERENCES

(1) Merz, K. M. Molecular dynamics simulations of lipid bilayers. *Curr. Opin. Struct. Biol.* **1997**, *7* (4), 511.
(2) Berkowitz, M. L.; Bostick, D. L.; Pandit, S. A. Aqueous Solutions next to Phospholipid Membrane Surfaces: Insights from Simulations. *Chem. Rev.* **2006**, *106* (4), 1527.
(3) Frey, S.; Tamm, L. K. Orientation of melittin in phospholipid bilayers. *Biophys. J.* **1991**, *60*, 922.
(4) Ludtke, S. J.; He, K.; Heller, W. T.; Harroun, T. A.; Yang, L.; Huang, H. W. Membrane pores induced by magainin. *Biochemistry* **1996**, *35*, 13723.
(5) Xiang, T.; Anderson, B. D. Liposomal drug transport: a molecular perspective from moleculardynamics simulations in lipid bilayers. *Adv. Drug Delivery Rev.* **2006**, *58*, 1357.
(6) Scott, R. W.; DeGrado, W. F.; Tew, G. N. De Novo Designed Synthetic Mimics of Antimicrobial Peptides. *Curr. Opin. Biotech.* **2008**, *19*, 620.
(7) Brunner, J.; Graham, D. E.; Hauser, H.; Semenza, G. Ion and Sugar Permeabilities of Lecithin Bilayers: Comparison of Curved and Planar Bilayers. *J. Membr. Biol.* **1980**, *57*, 133−141.
(8) Nichols, J. W.; Deamer, D. W. Net proton-hydroxyl permeability of large unilamellar liposomes measured by an acid-base titration technique. *Proc. Nat. Acad. Sci. U. S. A.* **1980**, *77* (4), 2038.
(9) Hauser, H. D.; Phillips, M. C. Mechanism of ion escape from phosphatidylcholine and phosphatidylserine single bilayer vesicles. *Biochemistry* **1973**, *12* (22), 4507.
(10) Kuyper, C. L.; Kuo, J. S.; Mutch, S. A.; Chiu, D. T. Proton permeation into single vesicles occurs via a sequential two-step mechanism and is heterogeneous. *J. Am. Chem. Soc.* **2006**, *128*, 3233.
(11) Matsuzaki, K.; Yoneyama, S.; Miyajima, K. Pore formation and translocation of melittin. *Biophys. J.* **1997**, *73*, 831.
(12) Ambroggio, E. E.; Bowie, F. J.H.; Fidelio, G. D.; Bagatolli, L. A. Direct visualization of membrane leakage induced by the antibiotic peptides: maculatin, citropin, and aurein. *Biophys. J.* **2005**, *89* (3), 1874.
(13) Paula, S.; Volkov, A. G.; VanHoek, A. N.; Haines, T. H.; Deamer, D. W. Permeation of protons, potassium ions, and small polar molecules through phospholipid bilayers as a function of membrane thickness. *Biophys. J.* **1996**, *70*, 339.
(14) Khavrutskii, I. V.; Gorfe, A. A.; Lu, B.; McCammon, J. A. Free energy for the permeation of Na^+ and Cl^- ions and their ion-pair through a zwitterionic dimyristoyl phosphatidylcholine lipid bilayer by umbrella integration with harmonic fourier beads. *J. Am. Chem. Soc.* **2009**, *131*, 1706.
(15) Torrie, G. M.; Valleau, J. P. Nonphysical sampling distributions in Monte Carlo free energy estimation - Umbrella sampling. *J. Comput. Phys.* **1977**, *23*, 187.
(16) Tepper, H. L.; Voth, G. A. Mechanisms of passive ion permeation through lipid bilayers: insights from simulations. *J. Phys. Chem. B* **2006**, *110*, 21327.
(17) Li, L.; Vorobyov, I.; Allen, T. The role of membrane thickness in charged protein−lipid interactions. *Biochim. Biophys. Acta* **2012**, *1818*, 135−145.
(18) Li, L.; Vorobyov, I.; Allen, T. The Different Interactions of Lysine and Arginine Side Chains with Lipid Membranes. *J. Phys. Chem. B* **2013**, *117*, 11906−11920.
(19) MacCallum, J. L.; Bennett, W. F. D.; Tieleman, D. P. Transfer of Arginine into Lipid Bilayers Is Nonadditive. *Biophys. J.* **2011**, *101*, 110−117.
(20) MacCallum, J. L.; Bennett, W. F. D.; Tieleman, D. P. Partitioning of Amino Acid Side Chains into Lipid Bilayers: Results from Computer Simulations and Comparison to Experiment. *J. Gen. Physiol.* **2007**, *129* (5), 371−377.
(21) Dorairaj, S.; Allen, T. W. On the thermodynamic stability of a charged arginine side chain in a transmembrane helix. *Proc. Nat. Acad. Sci. U. S. A.* **2007**, *104* (12), 4943.
(22) Huang, K.; García, A. E. Free energy of translocating an arginine-rich cell-penetrating peptide across a lipid bilayer suggests pore formation. *Biophys. J.* **2013**, *104*, 412−420.
(23) Tieleman, D. P.; Marrink, S. J. Lipids out of equilibrium: Energetics of desorption and pore mediated flip-flop. *J. Am. Chem. Soc.* **2006**, *128* (38), 12462.
(24) Sapay, N.; Bennett, W. F. D.; Tieleman, D. P. Thermodynamics of flip-flop and desorption for a systematic series of phosphatidylcholine lipids. *Soft Matter* **2009**, *5*, 3295.
(25) Bennett, W. F. D.; Tieleman, D. P. Water Defect and Pore Formation in Atomistic and Coarse-Grained Lipid Membranes: Pushing the Limits of Coarse Graining. *J. Chem. Theory Comput.* **2011**, *7*, 2981−2988.
(26) Wohlert, J.; Den Otter, W. K.; Edholm, O.; Briels, W. J. Free energy of a transmembrane pore calculated from atomistic molecular dynamics simulations. *J. Chem. Phys.* **2006**, *124*, 154905.
(27) Bennett, W. F. D.; MacCallum, J. L.; Tieleman, D. P. Thermodynamic Analysis of the Effect of Cholesterol on Dipalmitoyl-phosphatidylcholine Lipid Membranes. *J. Am. Chem. Soc.* **2009**, *131*, 1972−1978.
(28) Sapay, N.; Bennett, W. F. D.; Tieleman, D. P. Molecular Simulations of Lipid Flip-Flop in the Presence of Model transmembrane Helices. *Biochemistry* **2010**, *49*, 7665−7673.
(29) Deng, Y.; Roux, B. Hydration of Amino Acid Side Chains: Nonpolar and Electrostatic Contributions Calculated from Staged Molecular Dynamics Free Energy Simulations with Explicit Water Molecules. *J. Phys. Chem. B* **2004**, *108*, 16567.
(30) Li, L.; Vorobyov, I.; Allen, T. W. Potential of mean force and pKa profile calculation for a lipid membrane-exposed arginine side chain. *J. Phys. Chem. B* **2008**, *112* (32), 9574.
(31) Neale, C.; Madill, C.; Rauscher, S.; Pomés, R. Accelerating Convergence in Molecular Dynamics Simulations of Solutes in Lipid Membranes by Conducting a Random Walk along the Bilayer Normal. *J. Chem. Theory Comput.* **2013**, *9*, 3686−3703.
(32) Neale, C.; Bennett, W. F. D.; Tieleman, D. P.; Pomés, R. Statistical Convergence of Equilibrium Properties in Simulations of Molecular Solutes Embedded in Lipid Bilayers. *J. Chem. Theory Comput.* **2011**, *7*, 4175−4188.
(33) De Vries, A. H.; Mark, A. E.; Marrink, S. J. Molecular dynamics simulation of the spontaneous formation of a small DPPC vesicle in water in atomistic detail. *J. Am. Chem. Soc.* **2004**, *126*, 4488−4489.
(34) Marrink, S. J.; Lindahl, E.; Edholm, O.; Mark, A. E. Simulation of the spontaneous aggregation of phospholipids into bilayers. *J. Am. Chem. Soc.* **2001**, *123*, 8638−8639.
(35) E, W.; Vanden-Eijnden, E. Towards a theory of transition paths. *J. Stat. Phys.* **2006**, *123*, 503.
(36) E, W.; Ren, W.; Vanden-Eijnden, E. Minimum action method for the study of rare events. *Commun. Pure Appl. Math.* **2004**, *57* (5), 637−656.
(37) Melikov, K. C.; Frolov, V. A.; Shcherbakov, A.; Samsonov, A. V.; Chizmadzhev, Y. A. Voltage-induced nonconductive pre-pores and metastable single pores in unmodified planar lipid bilayer. *Biophys. J.* **2001**, *80*, 1829.
(38) Evans, E.; Heinrich, V.; Ludwig, F.; Rawicz, W. Dynamic tension spectroscopy and strength of biomembranes. *Biophys. J.* **2003**, *85*, 2342.
(39) Hess, B.; Kutzner, C.; Van Der Spoel, D.; Lindahl, E. GROMACS 4: Algorithms for Highly Efficient, Load-Balanced, and Scalable Molecular Simulation. *J. Chem. Theory Comput.* **2008**, *4*, 435.
(40) Ulmschneider, J. P.; Ulmschneider, M. B. United Atom Lipid Parameters for Combination with the Optimized Potentials for Liquid

Simulations All-Atom Force Field. *J. Chem. Theory Comput.* **2009**, *5*, 1803.
(41) Jorgensen, W. L.; Chandrasekhar, J.; Madura, J. D.; Impey, R. W.; Klein, M. L. Comparison of simple potential functions for simulating liquid water. *J. Chem. Phys.* **1983**, *79*, 926.
(42) Jorgensen, W. L.; Maxwell, D. S.; Tirado-Rives, J. Development and Testing of the OPLS All-Atom Force Field on Conformational Energetics and Properties of Organic Liquids. *J. Am. Chem. Soc.* **1996**, *118*, 11225.
(43) Darden, T.; York, D.; Pedersen, L. Particle mesh Ewald: An N·log(N) method for Ewald sums in large systems. *J. Chem. Phys.* **1993**, *98*, 10089.
(44) Hoover, W. G. Canonical dynamics: Equilibrium phase-space distributions. *Phys. Rev. A: At., Mol., Opt. Phys.* **1985**, *31* (3), 1695.
(45) Parrinello, M.; Rahman, A. Polymorphic transitions in single crystals: A new molecular dynamics method. *J. Appl. Phys.* **1981**, *52*, 7182.
(46) Kumar1, S.; Rosenberg1, J. M.; Bouzida, D.; Swendsen, R. H.; Kollman, P. A. The weighted histogram analysis method for free-energy calculations on biomolecules. I. The method. *J. Comput. Chem.* **1992**, *13*, 1011.